Mpala, SC, Gagnon, AS, Mansell, MG and Hussey, SW

The hydrology of sand rivers in Zimbabwe and the use of remote sensing to assess their level of saturation

Mpala, SC, Gagnon, AS, Mansell, MG and Hussey, SW

The hydrology of sand rivers in Zimbabwe and the use of remote sensing to assess their level of saturation

Highlights

- We investigate the influence of rainfall on the alluvial channels
- Important influence of the effective sediment depth and channel length on alluvial flow
- We investigate detection of water bearing sand rivers from satellite images.
- Landsat optical images showed alluvium extent and channel flooding and drying.
- There is potential to detect water bearing alluvial channels using ASAR images.

The hydrology of sand rivers in Zimbabwe and the use of remote sensing to assess their level of saturation

S.C. Mpala[a]; A.S. Gagnon[b, *]; M.G. Mansell[a]; S.W. Hussey[c]

[a] School of Engineering and Computing
University of the West of Scotland
High Street, Paisley PA1 2BE
Scotland, United Kingdom
mpala.sibonakaliso@uws.ac.uk
mamansell69@gmail.com

[b] Centre for Environmental Research
School of Science & Sport
University of the West of Scotland
High Street, Paisley PA1 2BE
Scotland, United Kingdom
Alexandre.Gagnon@uws.ac.uk

[c] Dabane Trust Water Workshops
P.O. Box 3331, Bulawayo
Zimbabwe
s.w.hussey@dabane.org

[*] Corresponding author. Tel: +44 (0) 141 848 3270; Fax: +44 (0) 848 3289; E-mail address: Alexandre.Gagnon@uws.ac.uk

ABSTRACT

Sand rivers are ephemeral watercourses containing sand that are occasionally flooded with rainwater runoff during the rainy season. Although the riverbed appears dry for most of the year, there is perennial groundwater flow within the sand. This water flowing beneath the surface is a valuable resource for local communities; nonetheless our understanding of such river systems is limited. Hence, this paper aims to improve our understanding of the hydrology of sand rivers and to examine the potential use of remote sensing to detect the presence of water in the sand. The relationship between rainfall events and changes in the water level of two sand rivers in the Matabeleland South Province of Zimbabwe was investigated. A lagged relationship was observed for the Manzamnyama River but for the Shashani River the relationship was seen only when considering cumulative rainfall events. The comparison of the modelled flow as simulated by a water balance model with observations revealed the important influence of the effective sediment depth on the recharge and recession of the alluvial channels in addition to the length of the channel. The possibility of detecting water in the alluvial sands was investigated using remote sensing. During the wet season, optical images showed that the presence of water on the riverbed was associated with a smooth signal, as it tends to reflect the incident radiation. A chronological analysis of radar images for different months of the year demonstrates that it is possible to detect the presence of water in the sand rivers. These results are a first step towards the development of a methodology that would aim to use remote sensing to help reducing survey costs by guiding exploratory activities to areas showing signs of water abstraction potential.

Keywords: Advanced synthetic aperture radar; alluvial aquifer; remote sensing; sand river; water level; Zimbabwe

1. Introduction

Sand rivers, also called *luggas* in East Africa and *wadis* in North Africa and the Middle East, are ephemeral watercourses containing sand, which are flooded with rainwater runoff once or a few times in a year (Herbert, 1998, Hussey, 1997, Nissen-Petersen, 1998). These rivers are the prevailing river type in the arid and semi-arid regions of southern Africa (Davies et al., 1994). Even though no water flows in the river bed for most of the year, there is perennial flow within the sand (Herbert, 1998). Figure 1 shows a typical sand river during the wet and dry season.

In southern Africa, particularly in Botswana and Zimbabwe, sand rivers are acknowledged as a potential source of drinking water, although their use is limited to a few small-scale water abstraction systems in remote rural communities. These sand water abstraction systems have the potential to augment supplies from established water supply systems, but have not been developed nor adopted by national water supply authorities (Hussey, 2007). Hence, water from sand rivers is not fully exploited in many areas where it could provide an essential source of water supply. For example, in 1998 it was estimated that there were approximately 900 km of sand rivers in Botswana with the potential to supply water to approximately a third of the country population at the time (Herbert, 1998). However, it is not clear what the size of the resource is in comparison with traditional surface and groundwater resources.

Shortly after a rainfall event, the water in a sand river recedes below the surface; nonetheless, it remains accessible by digging up to a certain depth (see Figure 1(c)), which depends on the time that elapsed since the end of the rainy season. Limited research has been conducted to date on the factors controlling the flow within the alluvium of ephemeral rivers. Love (2013) studied the influence of rainfall on the discharge of sand rivers in the Zhulube catchment of the northern Limpopo Basin of Zimbabwe. He observed that the recession after a rainfall event is typically short, in the order of a few days, and is caused by the rapid drying out of the shallow soils. The recesssion time was found to be longer, however, subsequent to larger floods caused by intense precipitation. For these reasons, he identified soil types and rainfall intensity as the two main factors influencing the recession time of a sand river. Mansell and Hussey (2005) also noted the influence of rainfall intensity on the recession time of a sand river but found that the flow velocity within the alluvium and the plan area of the channel were also important factors.

In Zimbabwe, sand rivers are increasingly used by non-governmental organisations (NGOs) to provide water in water stressed communities. The suitability of a sand river for effective and reliable abstraction of water depends on its gradient, width of the channel, the depth and grading of sediment, as well as the permeability and porosity of the soil. Hence, before a sand river is selected for water abstraction extensive appraisals, incorporating topographical surveys and GPS mapping, and probing and analysis of sediments have to be carried out. Such surveys can be costly and out of reach to many NGOs. The use of remote sensing to identify sand rivers showing signs of water abstraction potential could potentially reduce survey costs by guiding ground surveys to areas having shown signs of potential.

This paper comprises two objectives. The first objective aims to improve our understanding of the hydrology of sand rivers by presenting water level measurements taken on two rivers situated in the semi-arid region of south-western Zimbabwe, and to demonstrate how the water level in the sand rivers is related to rainfall and the characteristics of the river channel and catchment.

Continuous daily monitoring of the water level in a sand river using remote logging devices has not been previously done at the scale presented here. Research has to date been limited to direct measurements taken by research assistants, hence bringing in human error and inconsistencies, but which are eliminated by the accuracy and precision of a well calibrated water-level logger. The second objective is to examine the potential use of remote sensing to identify river channels with significant sediment deposits and to detect the presence of water within the alluvium. Previous research has shown the potential for using optical and radar images in feature identification and moisture detection, respectively, in different land cover types, but the usefulness of remote sensing to detect water in sand rivers has yet to be determined.

In the early 1980s detection of underground water was shown to be possible through long wave radar such as carried by the Shuttle Imaging Radar (SIR) systems, although the detection was only up to a few metres. Penetrations up to 6 m were documented at a 23.5 cm wavelength under ideal conditions (Elachi et al., 1984). In general, for penetration to occur the overlying material must be less than 2 m thick, the moisture content must be very low, and the surface must be rough to generate enough backscatter of the radar signal (Ford et al., 1989).Very few areas in the world are able to meet these conditions and this method is limited to buried river channels in the deserts of North Africa and the Middle East (Abdelsalam et al., 2000).

Another possibility to detect underground water remotely is through heat detection, as saturated soils have a greater heat capacity than dry soils (Becker, 2006). Thus, groundwater can be detected by large-scale thermal infrared (TIR) imagery because the relatively warm groundwater, especially at night, provides a contrast with the cool soil temperatures (Heilman and Moore, 1982).

2. Study Area

The ephemeral river systems presented in this study, i.e., the Manzamnyama and Shashani rivers, are both located in the Matabeleland South Province of southwestern Zimbabwe (Figure 2). The two rivers were chosen as they are currently sustaining small-scale sand water abstraction systems installed by the Dabane Trust**.** The Manzamnyama (or Nata) River flows in both Zimbabwe and Botswana; it is 330 km long from its source to mouth, 210 km of which are in Zimbabwe and 120 km in Botswana, and its total catchment area is 24,585 km^2. The river originates in a small farming town named Sandown located on the Zimbabwean central watershed 50 km south west of Bulawayo and ends in the Makgadikgadi saltpans of Botswana.

Field visits together with analyses of high-resolution satellite images show that the upper reaches of the Manzamnyama River are located in a commercial farming area where the Mananda Dam, a major dam on the Manzamnyama River, is located. Measurements of geo-referenced and ortho-rectified satellite images in a geographical information system (GIS) have shown that significant sedimentation begins to occur about 65 km along the river course marking the beginning of a 90 km stretch where the river passes through communal farming areas. It is on this stretch where the water abstraction potential of the ephemeral river is realised with communities relying on this water resource for domestic usage as well as for small-scale gardening and livestock farming. Hence, the current research focuses on this 90 km long section of the Manzamnyama River.

The Shashani River is a major tributary of the Shashe River. Like the Manzamnyama River, the Shashani River originates in the town of Sandown, but flows south (Figure 2). The Shashani River is 206 km long; it also a multi-faceted river, being used for commercial water supply for the upper half of its length and for communal water supply through sand water abstraction for the remainder of its course. In the commercial areas the Shashani River is dammed at two locations. The Shashani Dam is located about 37 km from the river source while the Gulati Dam is situated 55 km downstream from the first dam. The Shashani Dam was constructed to augment water supply to the Gulati Dam, which supplies water to the Antelope Estate and Irrigation Scheme owned by the Agricultural and Rural Development Authority (ARDA) (Gono, 2005). Most water abstraction on the sand river is currently practised on an undammed 50 km stretch of the river, beginning about 5 km downstream of the Gulati Dam and ending on its entry into a conservancy zone, 65 km from its mouth into the Shashe River. The current research was conducted on this stretch of river.

Both study sites are located in the middleveld region of the watershed plateau, a grassland region of intermediate altitude. The middleveld has a subtropical climate, experiencing one rainy season per year, which extends, on average, from late October to early April. Nonetheless, most precipitation falls between November and March, with total annual precipitation averaging around 450 mm. Rainfall in this region is erratic; it is characterised by long dry spells (Mansell and Hussey, 2005), with a few intense storms of short duration contributing to most of total annual precipitation (Edwards et al., 1983). Hussey (2007) showed how hot and dry areas with long periods without any rainfall have conditions prone to the formation of sand rivers as the incomplete weathering processes result in coarse sediment filling up river channels and retaining water in the pore spaces. For this reason, most rivers that originate in the middleveld are ephemeral. Ephemeral rivers are also found in the arid lowveld region where total annual precipitation reaches only 300 mm. This is in contrast to the higher altitude highveld region, which receives up to 1200 mm of rainfall annually and where perennial rivers are found (Vincent et al., 1960), but which covers only a small surface area of the country (Moyo, 1991).

Apart from major cities that rely on reservoirs for their water supply, most of the country relies on groundwater sources. Most of tropical Africa is underlain by crystalline basement rocks and the weathered overburden of these rocks functions as an aquifer, although the yields are typically only 20-60 $m^3 \bullet day^{-1}$ (Chilton and Foster, 1995). The depth of groundwater varies across the basement aquifer, but in many cases wells up to 20 m in depth are required. However, in the dry Matabeleland region of Zimbabwe, the water table is typically between 50 and 70 m below ground level (Lovell et al., 1994). At such depths, the water is usually saline, with salinity levels measured by the authors as high as 2000 ppm. For people in these regions, a more accessible and palatable water source are the sand beds of the ephemeral rivers, which provide a valuable source of relatively clean water without expensive drilling (Mansell and Hussey, 2005).

3. Materials and Methods

The project involved the collection of water level and climatic data as well as geomorphological characteristics of the two river channels, with a water balance model used to simulate the flow within the alluvial sands of the two rivers. In addition, remotely sensed data were obtained to determine the possibility of detecting water in the sand rivers.

3.1 Water level data

Water level data were collected from two loggers positioned in piezometers installed on the Manzamnyama and Shashani rivers during the period November 2009 to December 2010 and October 2012 to May 2013, respectively. The loggers were set to record water level on an hourly basis during the rainy season so as to capture the potentially rapid change in water level occurring at that time of the year (Mansell and Hussey, 2005). During the dry season, the recording interval was reduced to once a day at 8 am, as the change in water level is usually slow and gradual during that season. The sensor was installed within the alluvium (Figure 3), at the lowest estimated depth that the water level reaches annually, which is normally just before the onset of the rainy season in October. The sensor was linked by a waterproof data cable to an automatic logger installed on a pedestal on the riverbank. Testing was then done to ensure that the water level logger was properly installed. The water level data were downloaded from each logger during site visits that took place every two to three months.

3.2 Climatic data

Herbert et al. (1997) and Mansell and Hussey (2005) showed that rainfall is the main variable affecting the recharge of the sand rivers while Mansell and Hussey (2005) also noted that evaporation had a significant influence on the aquifer discharge when the water level is above or very close to the surface of the alluvium. In this paper, recharge refers to an increase in water level as a result of water reaching the saturated zone, notably following a rainfall event, but also as a result of the horizontal flow of water underneath the surface from upstream; while discharge refers to a decrease in water level. Hence, rainfall and temperature (the latter affecting evaporation) were the two climatic variables assumed to affect the most the water level within the alluvium. Daily rainfall and temperature data were obtained from a weather station situated in Plumtree for the period November 2009 - December 2010. The Plumtree is situated 60 km from the research site on one of the tributaries of the Manzamnyama River (Figure 2). Data were also obtained from Antelope Mine in Maphisa, which is on the banks of the Shashani River about 30 km upstream from the research site, for the period October 2012 - May 2013.

3.3 Water balance model

3.3.1 Model description

This study used the water balance model described in Mansell and Hussey (2005) to investigate how the water level in the sand rivers is related to rainfall and the characteristics of the river channel and catchment. It is a parametric model of intermediate complexity based on statistical averaging of the main hydrological processes that has been specially developed for modelling sand rivers. In the model, a change in water level Δh over a given period Δt is simulated according to the following equation:

$$A\Delta h/n = q\Delta t + q_a\Delta t + EA\Delta t - q_{rech}\Delta t \qquad (1)$$

where q, q_a, and q_{rech} are the outflow, abstraction, and recharge flows, respectively, A is the surface area of the channel, E is the evaporation depth, and n is the porosity of the sand.

The model consists of 17 parameters (Table 1), with the channel width, depth of sediment, and the initial water level collected during field research on the studied rivers in May 2014. The values of the other parameters were as reported in Mansell and Hussey (2005). The width of the channels was measured using a tape measure and verified by stadia tacheometry using an automatic level. Stadia tacheometry uses the readings of the top and bottom stadia of a levelling device, which is then multiplied by a given factor to get the distance between the machine and the point being sighted (Elhassan and Ali, 2011). GPS references of all levelling stations and random coordinates of the edges of alluvium deposition were also collected to assist with mapping the extent of the alluvial aquifer in a GIS.

Sand probing was used to measure the depth of sediment by inserting a six-metre long probing rod into the sand (Figure 4). Probing enables determination of the riverbed topography and when combined with levelling enables determination of the alluvial surface topography. During the insertion process, a marked resistance signalled that the probe had reached the bedrock or the clayey base of the riverbed. The initial water level was estimated by measuring the wet portion of the probe after it had been pulled out of the sand.

3.3.2 Model calibration

The Nash-Sutcliffe Efficiency (NSE) coefficient (Nash and Sutcliffe, 1970), the Root-Mean-Squared-Error (RMSE), and the Mean Absolute Error (MAE) were used to calibrate and validate the water balance model. The NSE coefficient is a popular metric for the calibration and validation of hydrologic models (Gupta et al., 2009, Afzal et al., 2015). It represents the ratio of the residual variance, i.e., the noise, to the variance of the observations, and is computed using the following equation:

$$NSE = 1 - \frac{\sum_{t=1}^{N}[O_t - P_t]^2}{\sum_{t=1}^{N}[O_t - \hat{O}]^2} \qquad (2)$$

where O_t and P_t are the observed and predicted water levels, respectively, at time *t*, while Ô is the mean of the observations (Yang et al., 2015). The values of the NSE cofficient can range from -∞ to one with a value closer to one referring to a more accurate model. A NSE coefficient of zero implies that the model predictions are as accurate as the mean of the observations and a negative coefficient indicates that the observed mean is better predictor than the model (Jain and Sudheer, 2008).

The RMSE measures the differences between the observed values and the values predicted by the model using the following equation:

$$RMSE = \sqrt{\frac{1}{n}\sum_{i=1}^{n} e_i^2} \qquad (3)$$

where *e* refers to the difference between the observed and predicted values at each time step in a time series of length *n*. The MAE represents the average of the absolute errors between the observations and the modelled values:

$$MAE = \frac{1}{n}\sum_{i=1}^{n}|e_i| \qquad (4)$$

(Chai and Draxler, 2014). Both the RMSE and the MAE can range from zero to ∞; the smaller the RMSE and MAE, the better the model.

The calibration of the water balance model consisted of adjusting manually four of the model parameters (highlighted in grey in Table 1) with the NSE coefficient used as an indicator of the accuracy of the resulting model. The calibration followed a three-step iterative procedure involving macro-level calibration, sensitivity analysis, and micro-level calibration, which was adapted from the seven-step process proposed by Ormsbee and Lingireddy (1997) for calibrating hydraulic networks. Macro-level calibration removes the most obvious errors, especially those due to estimated values being based on inaccurate assumptions. A sensitivity analysis helps to determine the variables that have the greatest impact on the model output. The analysis consisted of varying by ±20% the value of each of the model inputs and calculating the change in the model output resulting from that change (Hamby, 1995). Micro-level calibration is the final step in which the model is fine-tuned by making minute adjustments on variables that the model is most sensitive to.

3.4 Satellite images

Moyce et al. (2006) demonstrated the possibility of using Landsat images to identify the position of an alluvial river channel in south-western Zimbabwe. The current study is taking this further by examining the possibility of using those images to differentiate between rivers with and without any water on the riverbed. Optical images from the Landsat 8 satellite were obtained from the EarthExplorer website of the United States Geological Survey (USGS) (http://earthexplorer.usgs.gov/) over the study areas (Table 2). Interpretation of the Landsat images was based on supervised classification and analysis of natural look composites produced from Band 1, Band 2, and Band 3 of the multispectral images using the Spatial Analyst extension in ArcGIS.

The possibility of detecting water in the sand rivers through TIR imagery, as suggested in Becker (2006), could not be pursued. This is because TIR data at a spatial resolution finer than 30 m were not available for Zimbabwe. Further work was pursued using radar images, which, for the two studied alluvial channels, were available at a finer spatial resolution.

The radar images, captured by ASAR sensors aboard the Envisat satellite, were obtained from the European Space Agency (ESA) (Table 2). Envisat was launched in 2002 and the mission ended in April 2012 (European Space Agency, 2015). The researchers sought to determine if ASAR images were able to penetrate the unconsolidated dry sands of the two ephemeral rivers to produce an image of the subsurface and to relate the backscattering of that subsurface to the typical water content of the sand river at a given time of the year. For this purpose, the ASAR images were collected from different months during the hydrological year. However, because of the paucity of radar images over the studied areas, the images were not all from the most recent years but extended as far back as 2003.

The ASAR images were processed using the Next ESA Synthetic Aperture Radar (SAR) Toolbox (NEST), which is an open source toolbox for reading, processing, analysing, and visualising Envisat images, available from the ESA website (https://earth.esa.int/web/nest/home). NEST was used for radiometric calibration of the ASAR images so that the pixel values of the images truly represent the radar backscatter of the reflecting surface (Rosich et al., 2004). Radiometric correction also enables comparison of the images acquired with different sensors or acquired from the same sensor but at different times, in different modes, or processed by different processors (Li et al., 2008).

4. Results and Discussion

4.1. The relationship between water level and rainfall

Figure 5 depicts the water level measurements taken on the Shashani and the Manzamnyama rivers together with daily rainfall measurements. For the Shashani River this covers one rainy season. During that period there were a number of rainfall episodes, but the increase in water level within the sand river can only be seen for rainfall events producing at least 10 mm of rain. The cumulative effect of rainfall events occurring on consecutive days can also be observed and is associated with the highest water level peaks within the alluvium.

The water level on the Manzamnyama River and the associated rainfall measurements incorporate one hydrological year and the beginning of a second rainy season (Figure 5). In contrast to the Shashani River, the rise in water level on the Manzamnyama River is not gradual and occurs rather rapidly. For example, a 1.5 m rise in water level occurred within a matter of hours in both December 2009 and 2010. Although both rivers have dams upstream of the water level measurements, the difference in reservoir capacity as well as their management and operation is likely to explain the difference in the hydrograph of the Manzamnyama River in comparison with that of the Shashani River.

Storage dams alter river flows by storing water during storms and increasing flows during dry periods (McCully, 2001). For instance, the dam on the Manzamnyama River has a capacity of 11.45 million m^3 compared to a combined 30 million m^3 for the dams on the Shashani River. Even though it has a higher reservoir capacity, the Shashani River has a catchment area of 1400 km^2 with the two dams intercepting an upstream area of 670 km^2, which accounts for 47% of the catchment area. The catchment area of the Manzamnyama River is smaller at 2133 km^2 with the major dam intercepting only 346 km^2, which represents only 16% of the catchment area. Therefore, even though the catchment on the Shashani River is significantly smaller, it has greater reservoir storage capacity and a greater percentage of the catchment is dammed, thus giving the dams greater influence on the flows within the river system. The influence of the Mananda Dam on the Manzamnyama River at the research site is much smaller as it has a smaller reservoir capacity and impounds a smaller percentage of the catchment.

In a typical storm hydrograph, the peak runoff usually occurs sometime after the peak in rainfall. The lag time between the two peaks depends on the time of concentration, which is the time it takes for the river flow to reach the point being measured in the basin from the hydraulically most remote point in the watershed (Haan et al., 1994). The time of concentration depends on a number of factors, including the surface roughness, the shape and slope of the channel, and the flow pattern (Paulet et al., 1998). The size of the catchment area, the level of saturation of the soil, and rainfall intensity influence river discharge and consequently the peak of the runoff curve (Subramanya, 2013). Prolonged storms of low intensity contribute mostly to groundwater storage and produce relatively less runoff while high intensity storms over a small area increases the runoff because of minimised infiltration and evaporation losses (Soliman, 2011).

The hydrograph of the Shashani River shows that before mid-December most of the rainfall peaks have a corresponding increase in water level with a lag time of only a few days. Thereafter there is no clear pattern and only on a few occasions is a direct relationship between a rainfall event and an increase in water level seen. However, the cumulative impact of individual rainfall events is reflected in a clear and gradual increase in water level within the alluvium. This is possibly the result of sporadic episodes of convectional rains of high intensity extending over small areas, which prevail over Zimbabwe. These rainfall events are highly localised and consequently a rain gauge at a given weather station is unlikely to be representative of the whole catchment.

On the Shashani River, the water level, and thus the river discharge, is highest during the period January 16-21. In that period the water level, for the first time in that rainy season, water can be seen on the riverbed. This represents the period during which full recharge of the alluvium has taken place (Hussey, 1997), and is therefore a window during which optical images can be used to identify fully recharged ephemeral rivers through identification of surface flow.

4.2 Geomorphological characteristics of the channel

Figure 6 illustrates the profiles of two transects across the river about one kilometre apart on the lower reaches of the Shashani River at the confluence with the Shashe River, close to the location of the water level measurements. The profiles show that the top of the sand surface is not level and there are several undulations mostly influenced by movement of sand due to surface flow. As probing was done at the end of the rainy season, the water level is near the top of the sand. The water level is more uniform and subtle variations are likely due to human error.

4.3. Comparison of the modelled water level with observations

Table 1 shows how the model calibration improved the model fit for the two alluvial rivers. The model also performed well during the validation period as shown by the three indices (Table 3). The performance of the model is illustrated in Figure 7 for both the Shashani and Manzamnyama rivers. For the Shashani River the model reproduced very well the recession (i.e. discharge) trend during the dry season as well as some of the peaks associated with sand river recharge during the wet season. The modelled water level of the Manzamnyama River does not appear to be visually as good as that of the Shashani River. While the model does respond with an increased water level during the rainy season it did not reproduce well the discharge and recharge curves. The latter could be due to local variations in rainfall in different parts of the catchment. It was expected that the Shashani River be more unpredictable due to the effects of the upstream dams but the modelling results seem to prove otherwise. The limitation of the automatic logger used on the Manzamnyama River is also evident, as it only has a 1.5 m maximum water level recording, with the flattening out clearly seen in Figure 5 when the water level reaches 1.5 m. The same effect cannot be seen on the Shashani River where a newer logger with a higher range (0 – 5 m) was used.

4.4. The influence of the channel characteristics on the water level

The sensitivity analysis revealed that the length of the channel and depth of sediment were the two main model inputs affecting the accuracy of the modelled water level when compared to the actual measurements. The channel length, which is a ratio of the channel area to the actual width of the channel at the point being observed, is an indication of the length of the channel contributing to flow (Mansell and Hussey, 2005). Another observation of note was that the model better represented the water level measurements when the sediment depth in the model was equated to the difference between the highest water level and the lowest water level as opposed to the full sediment depth. This is referred to as the effective sediment depth, which can be determined by averaging of annual low and high water level observations for a given river.

4.5. Image Analysis

4.5.1. Optical images

On the optical images shown in Figure 8, the light coloured sands of the two ephemeral rivers stand out against the green tone of the vegetation and the yellow-brown tone of the land adjacent to the vegetation bordering the riverbed. The arrows in Figures 8(a) and 8(c) indicate the dry riverbeds of the Manzamnyama and Shashani Rivers, respectively. Figures 8(b) and 8(d) show the visible surface flow, which has fully submerged the two sand beds. Figure 9 is a high resolution Google Earth image of the Save River in Zimbabwe taken on April 16 2012, which is at the end of the rainy season. Although the image was not captured on any of the two rivers under investigation it gives a good illustration of the sand river identification potential of optical images. The image clearly shows differences in dry sand (labelled 1) and moist sand (labelled 2), while also showing vegetation cover (labelled 3) and bare ground cover (labelled 4).

Identifying a river with an extensive sand bed is the first stage in the process of selecting a sand river with the potential for a reliable abstraction of water. While there is no agreed standard for river width and sediment depth to define an extensive river bed, the work of Dabane Trust has recommended that a river be at least 20 m wide with a minimum sediment depth of 1.5 m. Hence, the second step is to determine the depth of the alluvium and the water level within the alluvium. Figures 8 and 9 show the extent of the alluvium and whether is river is saturated through the presence of water on the surface of the alluvium. The limitation of such optical images, however, is that they do not provide information about the depth of the alluvium. Traditionally, identifying a river with extensive alluvial deposition would require a river basin survey involving investigation of all known rivers. This long and expensive process is used to find rivers with the channel width, sediment depth, and longitudinal slope meeting the minimum requirements for sustainable water abstraction. Satellite images thus present an opportunity for surveyors to carry out desktop surveys and thus do field trips to verify rivers that have already been shortlisted through the desktop survey.

Images showing visible surface flow give an indication of high water level within the alluvium, as the presence of water on the riverbed indicates that the alluvium is saturated. The presence of moist sands on the optimal images should not lead to the immediate conclusion that the water table is high, however, as moist sands could also result from direct precipitation on the alluvium. For this reason, rainfall records would be useful and moisture that is detected remotely without a rainfall event having occurred in the last few days could then be attributed to high water levels within the alluvium.

To interpret moisture in optical images a reference image is required. This is because moisture alters the optical signature of the image, and the changes that moisture creates may not be distinguishable without an image depicting the *a priori* conditions. In Figure 9, moist sand was easier to pick out because the water did not fully wet the sand bed. Hence parts of the sand bed remained dry, giving the much required reference signature that led us to conclude that the other parts of the river channel were moist. The effect of moist sand on the recorded signature is more pronounced in radar images than optical images. Moisture in radar images has a more predictable signature; thereby radar images are more widely used to detect moisture than optical images.

4.5.2. Radar images

A radar image is usually displayed as a grey scale image. The intensity of each pixel represents the proportion of the microwave radiation that is backscattered by the surface. ASAR is an active sensor, meaning that it sends a radar signal to the surface area of the earth to be imaged and then records the signal that is reflected back to its sensor (Mather, 1999). This backscattering by the surface depends on a number of factors, notably the frequency and polarisation of the radar pulses; the incident angles of the radar beam; the types, sizes, shapes, and orientations of the scatterers in the target area; and the moisture content of the target area (Liew, 2001, European Space Agency, 2007). Depending on the texture of the target area, the signal can be reflected back to or away from the sensor, or even attenuated by trying to penetrate a loosely packed medium (Natural Resources Canada, 2003). If the signal is reflected back to the sensor the resulting image will be brighter whilst if it is attenuated or reflected away from the sensor a darker image results (Lacomme et al., 2001).

A smooth surface acts like a mirror for the incident radar pulse. Most of the incident radar energy is reflected away from the sensor with very little energy scattered back to the radar sensor (Figure 10(a)). A rough surface reflects the incident radar pulse in all directions and part of the radar energy is scattered back to the radar sensor (Figure 10(b)); hence a rough surface will appear brighter than a smooth surface on a radar image. For example, flat surfaces such as calm water normally appear as dark areas in a radar image since most of the incident radar pulses are reflected away in a specular way (Gupta, 2003, Liew, 2001). Considering a surface of the same roughness, when the soil is dry the incident radar energy is able to penetrate into the soil surface, resulting in less backscattered radar intensity (Figure 10(c), while for wet soils the large difference in electrical properties between water and air results in higher backscattered radar intensity (Figure 10(d)), and for flooded soils the radar is reflected in a specular way off the water surface, resulting in low backscattered intensity (Figure 10(e)). Hence the flooded area appears dark in the ASAR image. The interpretation of a radar image is not as straightforward as that of an optical image, however, and often requires some familiarity with the ground conditions of the areas being imaged (Liew, 2001).

Diffused reflection takes place when a rough surface reflects the incident radar radiation in all directions. When this occurs the amount of energy that is backscattered back depends the properties of the ground (Abdelsalam et al., 2000). For example, trees and other vegetation are usually moderately rough on the wavelength scale and consequently appear as moderately bright features in a radar image. The brightness of areas covered by bare soil may vary from very dark to very bright depending on its roughness and the moisture content of the soil. Dry rough soils will typically appear bright in a radar image and for a similar soil roughness; a surface with higher moisture content will appear brighter.

In January, during the peak of the rainy season, the moist river channel has a bright backscatter level, which is as high as the surrounding ground and vegetation, suggesting a moist but not flooded river channel (Figure 11(a)), and this continues until March at the end of the rainy season (Figure 11(b)). In both images, the river channel can still be seen and is indicated by arrow 1, 2 and 3. In Figure 11(a), arrows 1 and 2 point to the same river channel though presenting contrasting backscatter signatures. Arrow 1 shows a darker contrast associated with a flooded river channel while arrow 2 points to a brighter backscatter signature usually associated with moist sand. Arrow 3 in Figure 11(b) shows evidence of a moist river channel characterised by the high backscatter signature. Unlike in Figure 11(a) there is no surface water, and no part of the riverbed is submerged. There are subtle differences in backscatter intensity between Figures 11(a) and 11(b) resulting from differences in the level of moisture and vegetation cover at these two different times of the rainy season.

In June, during the winter dry season, which is two months after the cessation of the rains, the dry river channel shows high contrast with the vegetation (Figure 11(c)). This is because the backscatter coefficient of the river is lower than that of the vegetation canopy and the surrounding land, suggesting a dry river surface, and possible absorption of the radar signal by the presence of water located a few centimetres below the surface. The contrast is also relatively high in October just before the beginning of the rainy season (Figure 11(d)). On October 17 2003, the backscatter coefficient of the river, though lower than that of the vegetation canopy, is almost equal to that of the surrounding land suggesting a dry river surface, with characteristics similar to that of the surrounding land surface.

Figure 12 shows the variation in backscatter intensities of three different land-cover types.. These were extracted through radiometric calibration followed by supervised classification of the cover types and statistical averaging of the backscatter intensities from each of the classes. The average backscatter intensities show little variation over time for the vegetated land cover type. However, as we move from the wet months of February and March to the generally drier April, there is an increase in backscatter intensity for the sand showing a possible change from a submerged riverbed (low backscatter intensity) to a moist one (high backscatter intensity).

This chronological analysis of the ASAR images for different months of the year demonstrates that it is possible to detect moisture in the sand river channel as well as identifying a flooded river channel. However, the images do not have a long enough wavelength to penetrate the sands of the alluvial channel. ASAR uses radar images in the C-Band, which has a wavelength of 5.6 cm and a shorter penetration depth when compared to L-band, which has a wavelength of up to 30 cm and a penetration depth measured at more than 50% higher than that of C-band (Rignot et al., 2001). Penetration at greater depths were reported by Abdelsalam et al. (2000) and Elachi et al. (1984) using L-band radar although both their investigations were carried out under ideal conditions in the Sahara Desert.

5. Conclusions

This research investigated variations in flows in alluvial channels due to rainfall and compared water level measurements with values obtained from a water balance model calibrated using geomorphological data obtained during field research on the two alluvial channels. The data revealed that recharge of sand rivers is a very rapid process, which can occur within hours of a storm, while recession was a much slower process occurring over a number of months. This sponge effect of the alluvium enables it to act as a store for water, which is abstracted by the users until it all flows out. It was found that the length of the river channel contributing to the river flow and the effective sediment depth had an important effect on the recharge and recession of the alluvial channel.

The research has also shown the potential to detect water bearing alluvial channels using ASAR images. Our results show a change in backscatter intensity as a function of change in surface moisture level over time. It has also been possible to delineate the river channel using supervised classification and statistical averaging of the different backscatter intensities between vegetation cover (on the banks) and the coarse sand that makes up the river channel.

It was also necessary to have optical images to give a visual appraisal of the nature of the alluvium on the day in question. For this study, optical images and rainfall data were used to give an indication of inherent conditions. The optical images were particularly useful in determining if the actual channel has some alluvium on it, and also to determine if there was any surface flow or moisture. Rainfall data were used to determine days during which surface moisture was most likely to be present without necessarily indicating a higher water level within the sediment.

The results of these investigations present a new understanding of sand rivers while presenting relatively cheaper and faster ways of identifying the degree of saturation of sand rivers using satellite data. For a water supply system that is overshadowed by more prominent surface and groundwater supply options the cheaper identification and hydrological characterisation using a combination of free satellite remote sensing data and spread sheet based water balance modelling should help in promoting its uptake and trenching out to more communities in the semi-arid regions of Zimbabwe. Sand water abstraction has the potential to transform livelihoods and contribute to the socio-economic development of the rural communities of southern Africa. This would be by providing an alternative source of much needed water, which can be used to support not only life, but also food security and livelihoods through irrigation and livestock farming.

Further research will consist of testing the water balance model over a longer data range and different river systems to analyse its sensitivity to different climatic and geomorphological systems. Also, sand river detection using L-band radar images will be explored.

6. Acknowledgements

The authors acknowledge the Margaret Hayman Charitable Trust for funding the postgraduate studies of the first author. The authors also acknowledge support from the Dabane Trust and the Water Extraction Technologies Trust (WETT) for their financial support to the field research and travelling expenses. We also acknowledge the ESA for access to the restricted ASAR images and for making publicly available their analytical toolbox for processing their radar images publicly available. A.S. Gagnon acknowledges financial support from the Scottish Alliance for Geoscience, Environment and Society (SAGES).

7. Figure captions

Fig. 1. The Shashani River during the wet (left) and dry season (centre), and illustration of the depth of the water level during the dry season (right).

Fig. 2. Location of the two research sites and weather stations on the Manzamnyama and Shashani rivers in the Matabeleland South Province of Zimbabwe.

Fig. 3. Installation of a water level logger on the Shashani River (left and centre) and testing to ensure the logger is properly installed (right).

Fig. 4. Probing on the lower Shashani River.

Fig 5. Water level of the Shashani River (a) and Manzamnyama River (b), together with daily rainfall measurements from Antelope and Plumtree.

Fig. 6. Topographical survey at two locations on the Shashani River with the top transect situated one kilometre upstream from the bottom transect.

Fig. 7. Modelled and observed water level on the Shashani River (top) and Manzamnyama River (bottom).

Fig. 8. ***Top:*** Landsat images over the Manzamnyama River on November 28 2013 (left) showing a dry river channel and on December 23 2013 (right) showing a flooded river channel. ***Bottom:*** Landsat images over the Shashani River on December 22 2013 (left) showing a dry river channel and on January 7 2014 (right) showing a flooded river channel.

Fig. 9. Satellite image of part of the Save River in Zimbabwe showing differences in optical signatures between dry sand (1), moist sand (2), vegetation (3) and bare ground (4).

Fig. 10 Typical backscatter signature of a radar signal under a smooth (a) and rough (b) surface. Also shown is the typical backscattering signature for dry soils (c), wet soils (d), and flooded soils (e), considering a surface of the same roughness.

Fig. 11. Backscattering signature of the ASAR signal over the Manzamnyama River on January 31 2004 (a), March 31 2012 (b), June 18 2004 (c), and October 17 2003 (d). The arrows point to part of the river channel in all images. The read rectangle shows the study area.

Fig. 12. Variation in backscatter intensity for the different land cover types along the Manzamnyama River over time.

8. References

ABDELSALAM, M. G., ROBINSON, C., EL-BAZ, F. & STERN, R. J. 2000. Applications of orbital imaging radar for geologic studies in arid regions: The Saharan testimony. *Photogrammetric Engineering and Remote Sensing,* 66**,** 717-726.

AFZAL, M., GAGNON, A. S. & MANSELL, M. G. 2015. The impact of projected changes in climate variability on the reliability of surface water supply in Scotland. *Water Science & Technology: Water Supply,* 15**,** 736.

BECKER, M. W. 2006. Potential for satellite remote sensing of ground water. *Ground Water,* 44**,** 306-18.

CHAI, T. & DRAXLER, R. R. 2014. Root mean square error (RMSE) or mean absolute error (MAE)? – Arguments against avoiding RMSE in the literature. *Geoscientific Model Development,* 7**,** 1247-1250.

CHILTON, P. J. & FOSTER, S. S. D. 1995. Hydrogeological Characterisation And Water-Supply Potential Of Basement Aquifers In Tropical Africa. *Hydrogeology Journal,* 3**,** 36-49.

DAVIES, B. R., THOMS, M. C., WALKER, K. F., O'KEEFFE, J. H. & GORE, J. A. 1994. Dryland Rivers: Their Ecology, Conservation and Management. *The Rivers Handbook.* Oxford: Blackwell Science Ltd.

EDWARDS, K. A., CLASSEN, G. A. & SCHROTEN, E. H. J. 1983. THE WATER RESOURCE IN TROPICAL AFRICA AND ITS EXPLOITATION. *ILCA (International Livestock Centre for Africa) Research Report.* Addis Ababa, Ethiopia: International Livestock Centre for Africa.

ELACHI, C., ROTH, L. E. & SCHABER, G. G. 1984. Spaceborne Radar Subsurface Imaging in Hyperarid Regions. *IEEE Transactions on Geoscience and Remote Sensing,* GE-22**,** 383-388.

ELHASSAN, I. M. & ALI, A. S. 2011. Comparative study of accuracy in distance measurement using: Optical and digital levels. *Journal of King Saud University - Engineering Sciences,* 23**,** 15-19.

EUROPEAN SPACE AGENCY. 2007. *ASAR Product Handbook* [Online]. France: European Space Agency. Available: http://envisat.esa.int/handbooks/asar/CNTR.html.

EUROPEAN SPACE AGENCY. 2015. *ESA Earth Online 2000 - 2015* [Online]. Rome, Italy: European Space Agency (ESA). Available: https://earth.esa.int/web/guest/home [Accessed March 9 2015].

FORD, J. P., BLOM, R. G., CRISP, J. A., ELACHI, C., FARR, T. G., SAUNDERS, R. S., THEILIG, E. E., WALL, S. D. & YEWELL, S. B. 1989. Spaceborne radar observations: A guide for Magellan radar-image analysis Dec 15, 1989 ed. Pasadena, California: Jet Propulsion Laboratory, California Institute of Technology.

GONO, G. 2005. Drought mitigation and resuscitation policies for the agricultural sector in Zimbabwe. Supplement 2 of 3 to the 1st quarter monetary policy statement. Harare, Zimbabwe: Reserve Bank of Zimbabwe.

GUPTA, H. V., KLING, H., YILMAZ, K. K. & MARTINEZ, G. F. 2009. Decomposition of the mean squared error and NSE performance criteria: Implications for improving hydrological modelling. *Journal of Hydrology,* 377**,** 80-91.

GUPTA, R. P. 2003. *Remote Sensing Geology*, Springer.

HAAN, C. T., BARFIELD, B. J. & HAYES, J. C. 1994. *Design Hydrology and Sedimentology for Small Catchments*, London, United Kingdom, Academic Press Limited.

HAMBY, D. M. 1995. A comparison of sensitivity analysis techniques. *Health Phys,* 68**,** 195-204.

HEILMAN, J. L. & MOORE, D. G. 1982. Evaluating Depth to Shallow Groundwater Using Heat-Capacity Mapping Mission (Hcmm) Data. *Photogrammetric Engineering and Remote Sensing,* 48**,** 1903-1906.

HERBERT, R. 1998. Water from sand rivers in Botswana. *Quarterly Journal of Engineering Geology and Hydrogeology,* 31**,** 81-83.

HERBERT, R., BARKER, J. A., DAVIES, J. & KATAI, O. T. Exploiting Ground Water from Sand Rivers in Botswana using Collector Wells. *In:* JIN, F. & KROTHE, N. C., eds. Proceedings of the 30th International Geological Congress, 1997 Beijing, China. Utrecht, The Netherlands: VSP BV.

HUSSEY, S. W. Small-scale Sand Abstraction Systems. 23rd WEDC Conference Water and Sanitation for All, 1997 Durban. WEDC.

HUSSEY, S. W. 2007. *Water from Sand Rivers*.

JAIN, S. K. & SUDHEER, K. P. 2008. Fitting of Hydrologic Models: A Close Look at the Nash–Sutcliffe Index. *Journal of Hydrologic Engineering,* 13**,** 981-986.

LACOMME, P., HARDANGE, J.-P., MARCHAIS, J.-C. & NORMANT, E. 2001. The Radar Equation. *In:* LACOMME, P., HARDANGE, J.-P., MARCHAIS, J.-C. & NORMANT, E. (eds.) *Air and Spaceborne Radar Systems.* Norwich, NY: William Andrew Publishing.

LI, Z., CHEN, J. & BALTSAVIAS, E. 2008. *Advances in Photogrammetry, Remote Sensing and Spatial Information Sciences: 2008 ISPRS Congress Book*, CRC Press.

LIEW, S. C. 2001. *Principles of Remote Sensing* [Online]. Singapore: National University of Singapore. 2015].
LOVE, D. 2013. *Water Resources Strategies To Increase Food Production In The Semi-Arid Tropics: With Particular Emphasis On The Potential of Alluvial Groundwater.* PhD, Delft University of Technology.
LOVELL, C., MURATA, M., BROWN, M., BATCHELOR, C., CHILTON, P., SEMPLE, A., THOMPSON, D. & DUBE, T. 1994. Small scale irrigation using collector wells Pilot Project-Zimbabwe. *Fourth Progress Report. ODA Report,* 94.
MANSELL, M. G. & HUSSEY, S. W. 2005. An investigation of flows and losses within the alluvial sands of ephemeral rivers in Zimbabwe. *Journal of Hydrology,* 314**,** 192-203.
MATHER, P. M. 1999. *Computer Processing of Remotely Sensed Images An Introduction,* Chichester, West Sussex, England, John Wiley & Sons Ltd.
MCCAULEY, J. F., SCHABER, G. G., BREED, C. S., GROLIER, M. J., HAYNES, C. V., ISSAWI, B., ELACHI, C. & BLOM, R. 1982. Subsurface valleys and geoarcheology of the eastern sahara revealed by shuttle radar. *Science,* 218**,** 1004-20.
MCCULLY, P. 2001. *Silenced rivers: the ecology and politics of large dams*, Zed Books.
MOYCE, W., MANGEYA, P., OWEN, R. & LOVE, D. 2006. Alluvial aquifers in the Mzingwane catchment: Their distribution, properties, current usage and potential expansion. *Physics and Chemistry of the Earth, Parts A/B/C,* 31**,** 988-994.
MOYO, S. 1991. *Zimbabwe'e environmental dilemma: balancing resource inequities*, Zimbabwe Environmental Research Organisation.
NASH, J. E. & SUTCLIFFE, J. V. 1970. River flow forecasting through conceptual models part I — A discussion of principles. *Journal of Hydrology,* 10**,** 282-290.
NATURAL RESOURCES CANADA 2003. *Fundamentals of Remote Sensing*, Natural Resources Canada.
NISSEN-PETERSEN, E. 1998. *Water from sand-rivers*.
ORMSBEE, L. E. & LINGIREDDY, S. 1997. Calibrating Hydraulic Network Models (PDF). *Journal - American Water Works Association,* 89**,** 42-50.
PAULET, M., MARTE, R. J., RODRIQUEZ, F. T., PAYANO, T., PORTORREAL, M., MELO, H. & MORA, S. C. 1998. *Trip Report United States Department of Agriculture (USDA) Natural Resources Conservation Service (NRCS)*, Bib. Orton IICA / CATIE.
RANGO, A. 1994. Application of remote sensing methods to hydrology and water resources. *Hydrological Sciences Journal,* 39**,** 309-320.
RIGNOT, E., ECHELMEYER, K. & KRABILL, W. 2001. Penetration depth of interferometric synthetic- aperture radar signals in snow and ice. *Geophysical Research Letters*, 28**,** 3501-3504.
ROSICH, B., MEADOWS, P. & MONTI-GUARNIERI, A. ENVISAT ASAR product calibration and product quality status. Proc. CEOS SAR Workshop, 2004. Citeseer, 24-25.
SOLIMAN, M. M. 2011. *Engineering Hydrology of Arid and Semi-Arid Regions*, CRC Press.
SUBRAMANYA, K. 2013. *Engineering Hydrology,* New Delhi, McGraw Hill Education (India) Private Limited.
VINCENT, V., THOMAS, R. & STAPLES, R. 1960. An agricultural survey of Southern Rhodesia. Part 1. Agro-ecological survey. *An agricultural survey of Southern Rhodesia. Part 1. Agro-ecological survey.*

YANG, Q., WANG, Y., ZHANG, J. & DELGADO, J. 2015. A comparative study of shallow groundwater level simulation with three time series models in a coastal aquifer of South China. *Applied Water Science***,** 1-10.

Table 1

Table 1 Values of the water balance model parameters before and after calibration

Model Parameter	Shashani River		Manzamnyama River		Unit
	Initial	Calibrated	Initial	Calibrated	
Channel width	133	133	50	50	m
Initial velocity	0.6	1.3	0.4	0.4	m/day
Plan area of channel	39900	39900	12500	6000	m^2
Length of channel	0.3	0.3	0.25	0.12	km
Depth of sediment	1.5	1.5	1.5	1.5	m
Initial water level	0.2	0.2	1.5	1.5	m
Average pan evaporation	0.004	0.005	0.004	0.004	m/day
Abstraction	1.00	1.00	10.00	13.00	m^3/day
Sediment type	medium	medium	medium	medium	sand
Dry moisture content	0.1	0.1	0.1	0.1	
Saturated moisture content	0.4	0.4	0.4	0.4	
Deep water depth	2.9	1.5	1.5	1.5	m
Shallow water depth	0.1	0	0.1	0.1	m
Porosity	0.4	0.4	0.4	0.4	
Moisture exponent	2	2	2	2	m
Velocity exponent	0	0	0	0	
Catchment ratio	8	6	4	4	
NSE	-0.01	0.65	-3.90	0.87	
RMSE	0.32	0.17	0.46	0.13	m
MAE	0.27	0.13	0.38	0.09	m

Table 2

Table 2 Selected satellite images

IMAGE CAPTURE DATE & TIME	SATELLITE	SENSOR	IMAGE ID
17/10/2003 07:44	Envisat-1	ASAR/IM	ASA_IMP_1PNIPA20031017_074424_000000162020_00450_08520_0688
31/01/2004 07:47	Envisat-1	ASAR/IM	ASA_IMP_1PNIPA20040131_074713_000000162023_00221_09794_0635
18/06/2004 7:44	Envisat-1	ASAR/IM	ASA_IMP_1PNIPA20040618_074427_000000162027_00450_12027_0634
31/03/2012 07:54	Envisat-1	ASAR/IM	ASA_IMG_1PNUPA20120331_075453_000000163113_00150_52750_0654
27/11/2013 08:14	Landsat 8	OLI_TIRS	LC81720742013331LGN00
22/12/2013 08:08	Landsat 8	OLI_TIRS	LC81710752013356LGN00
23/12/2013 08:08	Landsat 8	OLI_TIRS	LC81710742013356LGN00
07/01/2014 08:08	Landsat 8	OLI_TIRS	LC81710752014007LGN00

Table 3

Table 3 Results of the calibration and validation of the water balance model on the Shashani and Manzamnyama rivers

	Shashani River		Manzamnyama River	
Efficiency Criteria	Calibration	Validation	Calibration	Validation
NSE	0.65	0.65	0.87	0.85
RMSE	0.17	0.07	0.13	0.16
MAE	0.13	0.04	0.09	0.14
Data time period	Oct '12 - May '13	May '14 - April '15	Jul '10 - Dec '10	Jul '11 - Dec '11

Figure 1

Figure 2

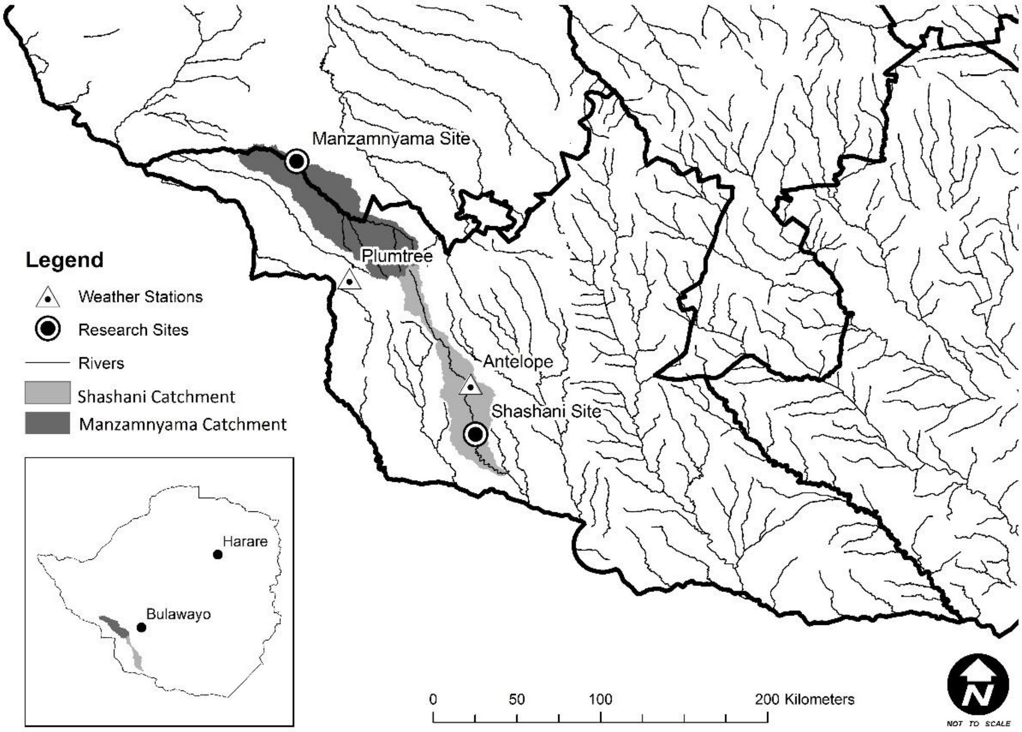
Manzamnyama Site
Plumtree
Antelope
Shashani Site
Legend
Weather Stations
Research Sites
Rivers
Shashani Catchment
Manzamnyama Catchment
Harare
Bulawayo
0
50
100
200 Kilometers
N
NOT TO SCALE

Figure 3

Figure 4

Figure 5

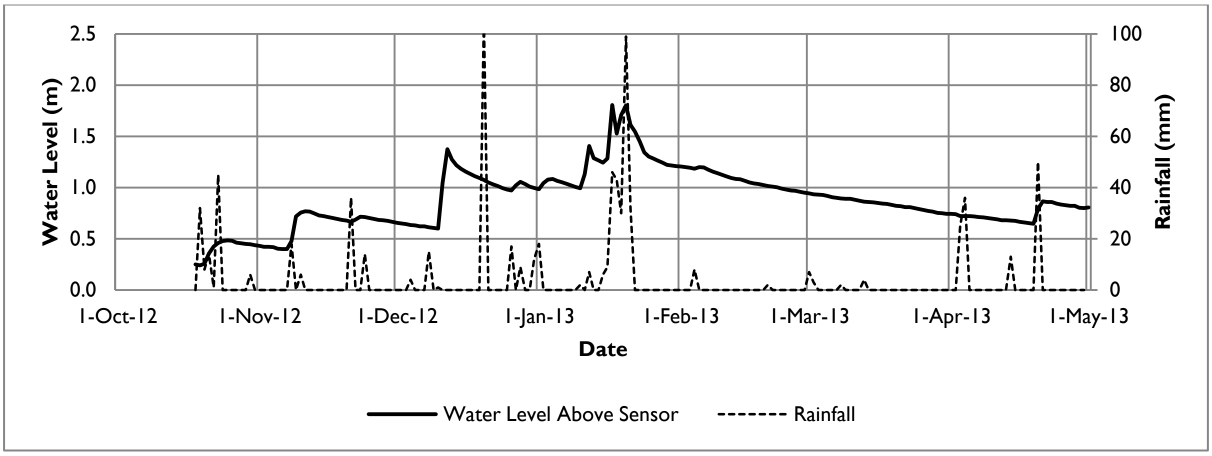

2.5
2.0
1.5
1.0
0.5
0.0
Water Level (m)
100
80
60
40
20
0
Rainfall (mm)
1-Oct-12
1-Nov-12
1-Dec-12
1-Jan-13
1-Feb-13
1-Mar-13
1-Apr-13
1-May-13
Date
Water Level Above Sensor
Rainfall

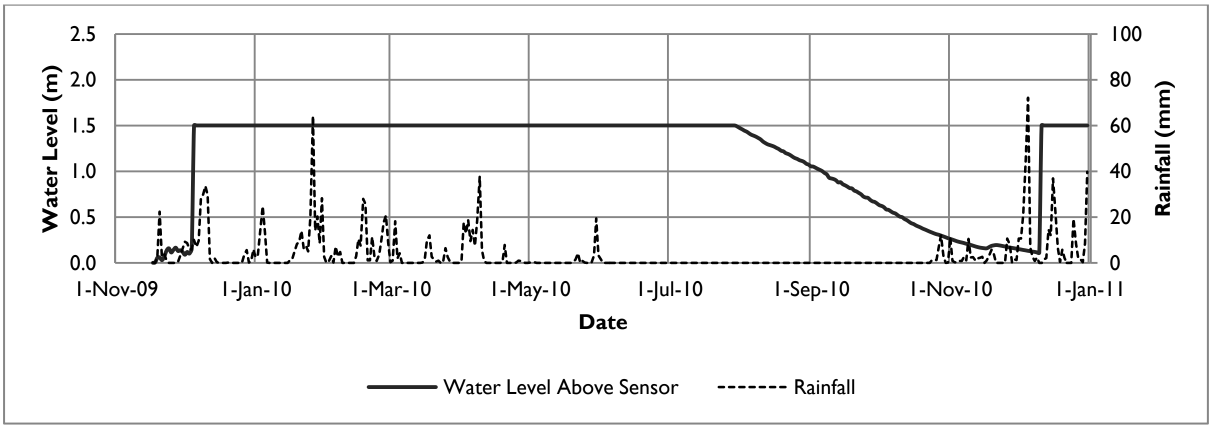

2.5
2.0
1.5
1.0
0.5
0.0
Water Level (m)
100
80
60
40
20
0
Rainfall (mm)
1-Nov-09
1-Jan-10
1-Mar-10
1-May-10
1-Jul-10
1-Sep-10
1-Nov-10
1-Jan-11
Date
Water Level Above Sensor
Rainfall

Figure 6

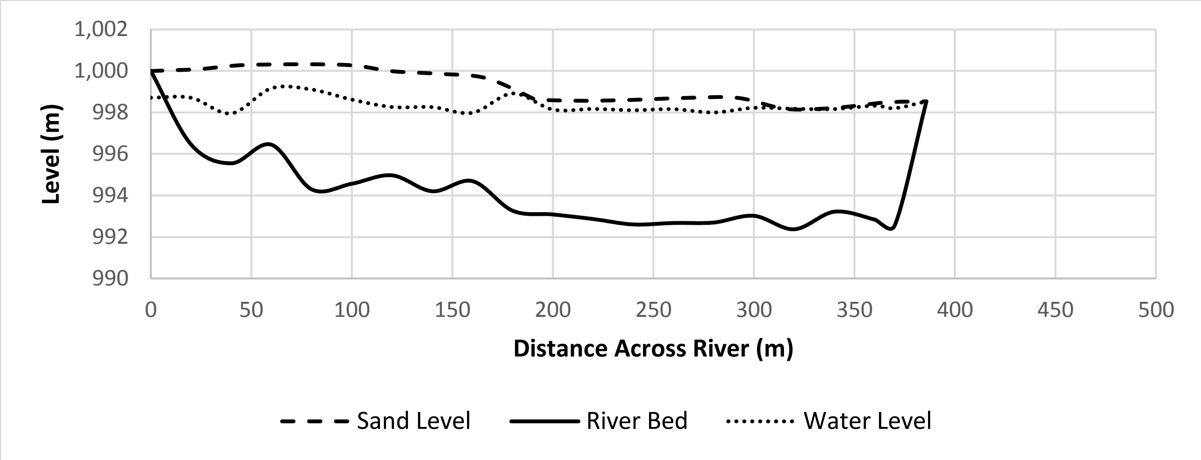

1,002
1,000
998
996
994
992
990
Level (m)
0
50
100
150
200
250
300
350
400
450
500
Distance Across River (m)
Sand Level
River Bed
Water Level

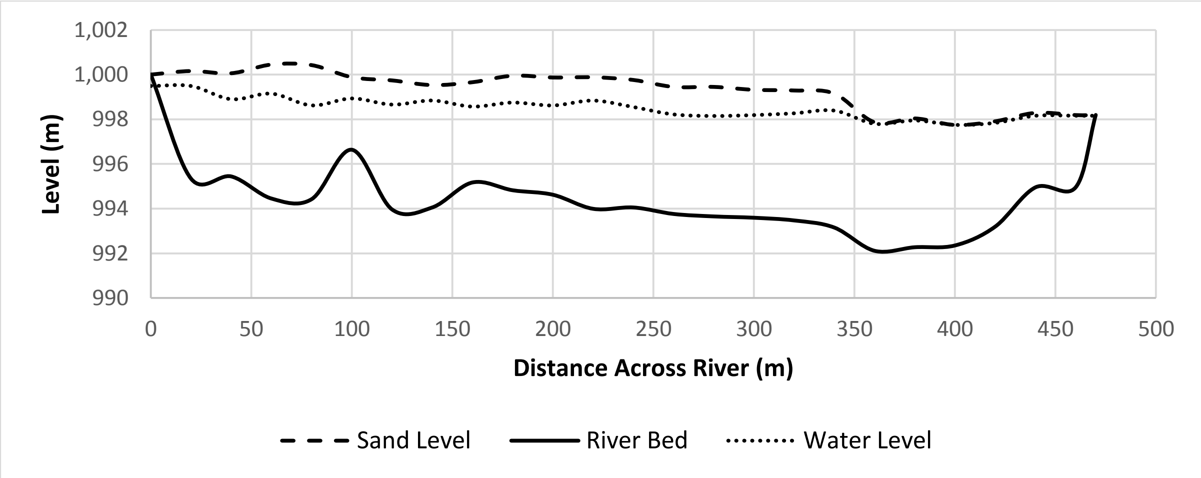

1,002
1,000
998
996
994
992
990
Level (m)
0
50
100
150
200
250
300
350
400
450
500
Distance Across River (m)
Sand Level
River Bed
Water Level

Figure 7

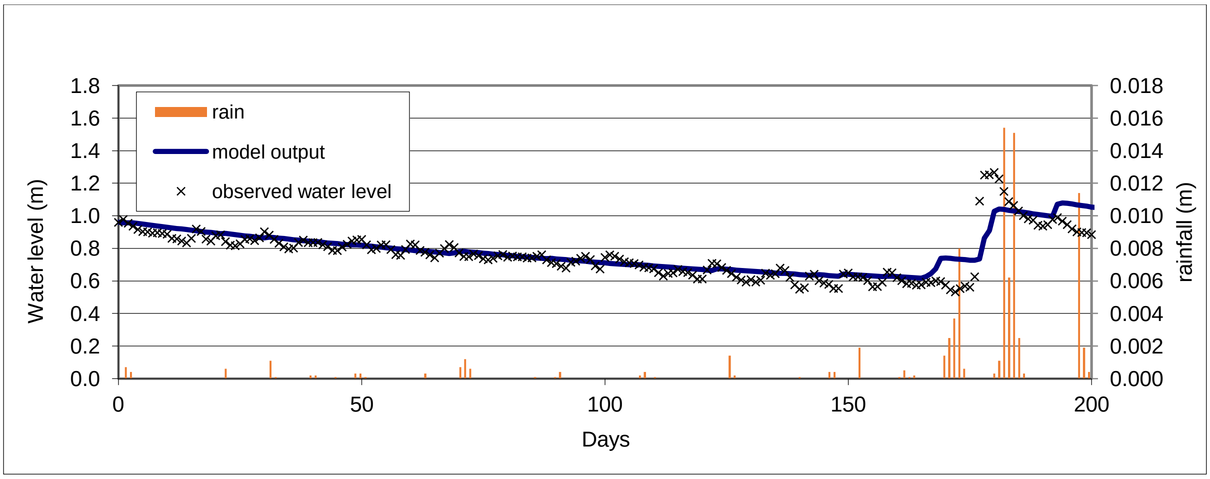

rain
model output
observed water level
Water level (m)
rainfall (m)
Days
1.8
1.6
1.4
1.2
1.0
0.8
0.6
0.4
0.2
0.0
0.018
0.016
0.014
0.012
0.010
0.008
0.006
0.004
0.002
0.000
0
50
100
150
200

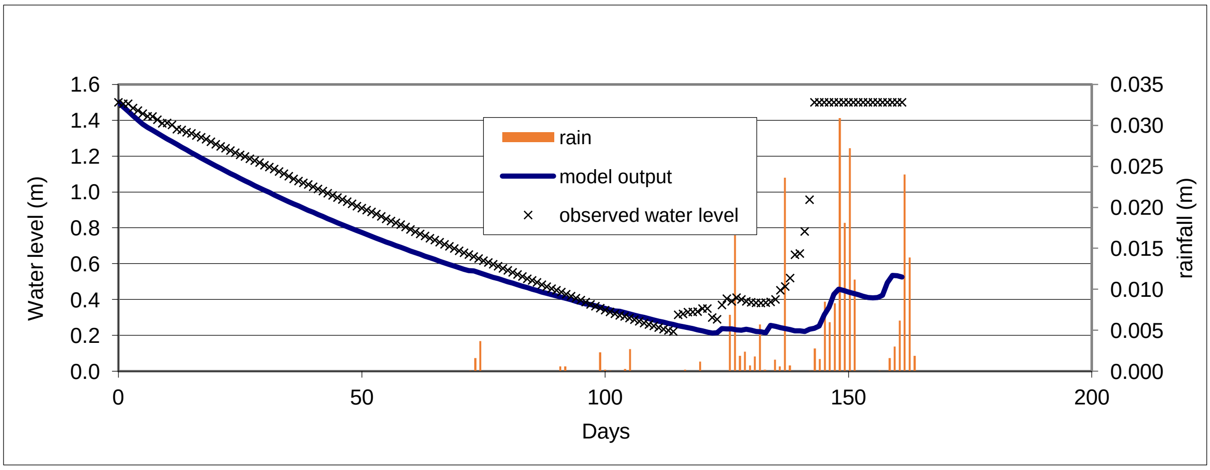

rain
model output
observed water level
Water level (m)
rainfall (m)
Days
1.6
1.4
1.2
1.0
0.8
0.6
0.4
0.2
0.0
0.035
0.030
0.025
0.020
0.015
0.010
0.005
0.000
0
50
100
150
200

Figure 8

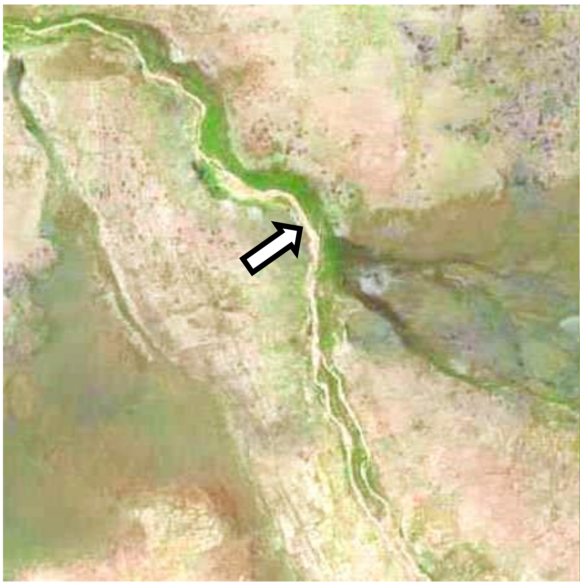

(a)

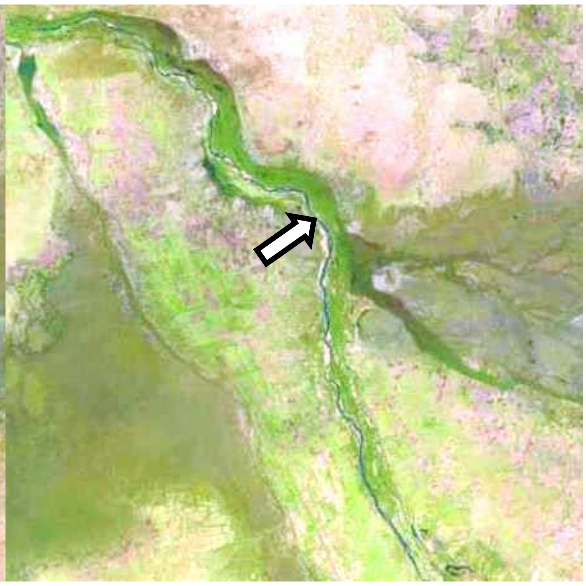

(b)

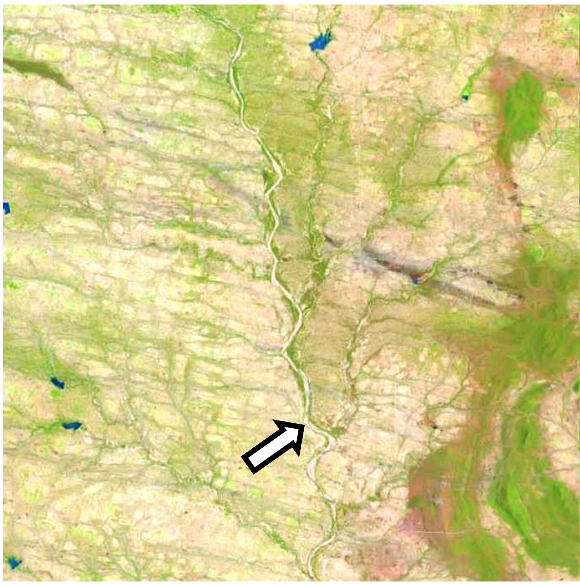

(c)

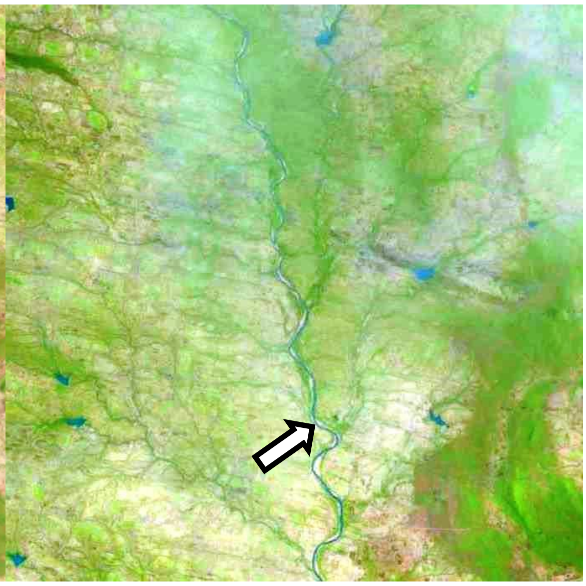

(d)

Figure 9

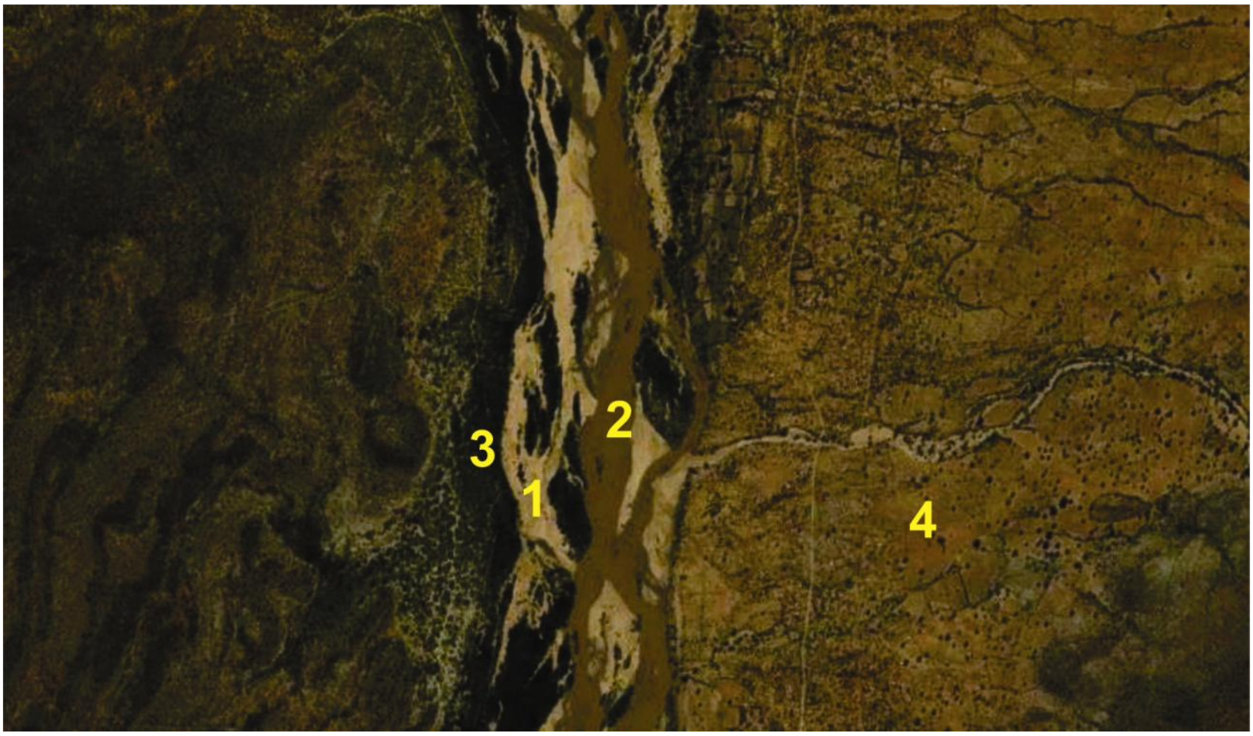

Figure 10

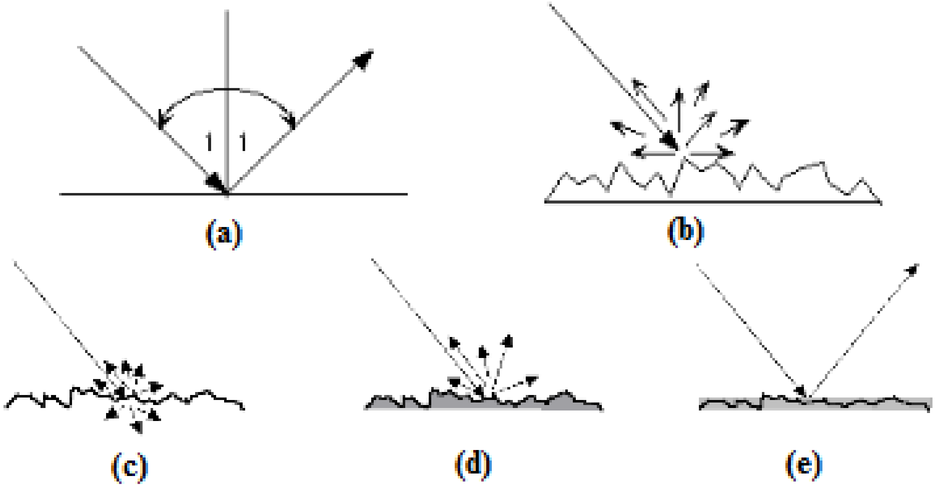

Figure 11

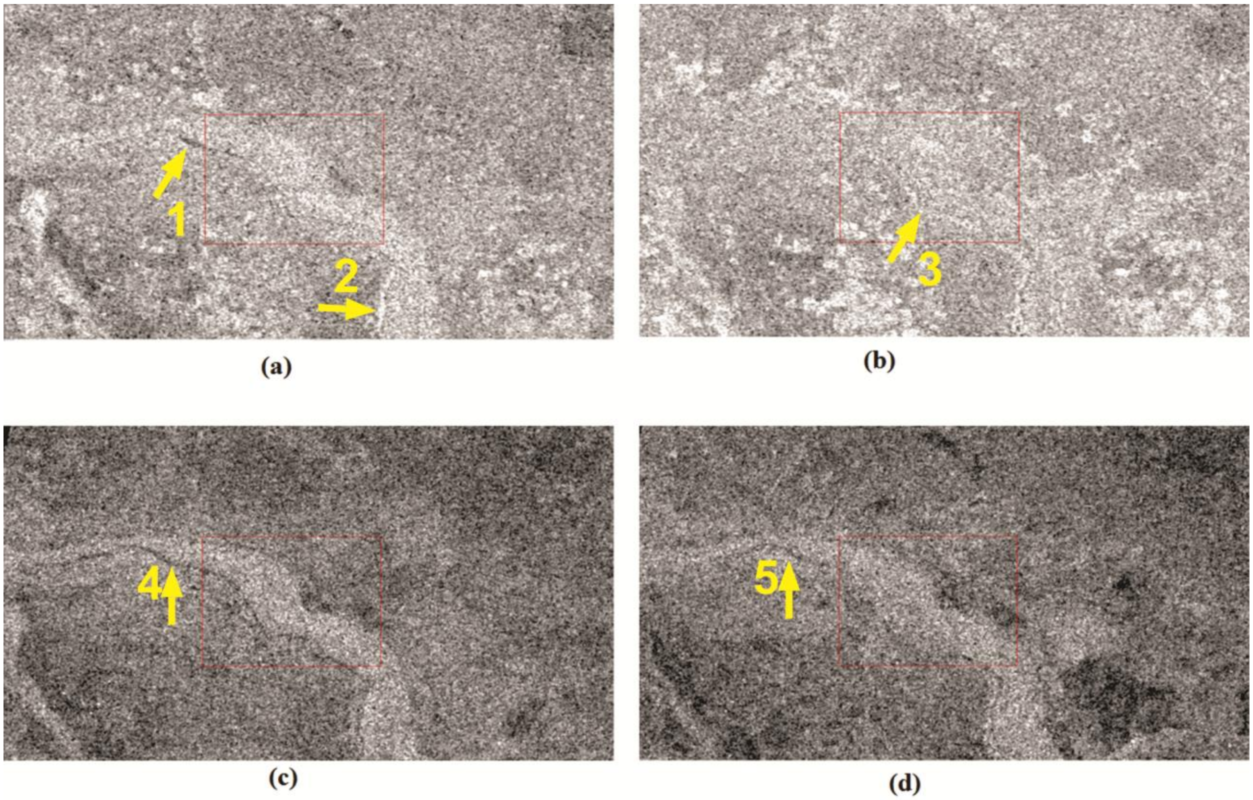

(a) (b)

(c) (d)

Figure 12

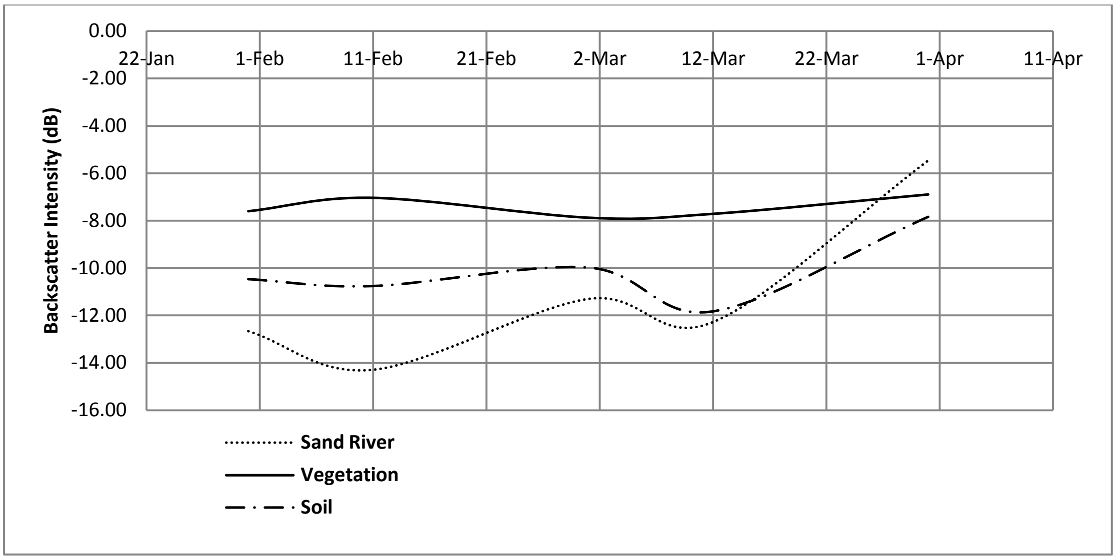

0.00
-2.00
-4.00
-6.00
-8.00
-10.00
-12.00
-14.00
-16.00
22-Jan
1-Feb
11-Feb
21-Feb
2-Mar
12-Mar
22-Mar
1-Apr
11-Apr
Backscatter Intensity (dB)
Sand River
Vegetation
Soil